ISSN 2070-0482, Mathematical Models and Computer Simulations, 2012, Vol. 4, No. 3, pp. 321–335. © Pleiades Publishing, Ltd., 2012.
Original Russian Text © M.K. Baev, G.G. Chernykh, 2011, published in Matematicheskoe Modelirovanie, 2011, Vol. 23, No. 10, pp. 44–64.

Numerical Model of a Turbulent Flow Behind a Heated Grid in a Wind Tunnel

M. K. Baev[a] and G. G. Chernykh[a, b, c]

[a] *Institute of Computational Technologies, Siberian Branch, Russian Academy of Sciences, Novosibirsk, 630090 Russia*
[b] *Siberian State University of Telecommunications and Information Systems, Novosibirsk, 630102 Russia*
[c] *Novosibirsk State University, Novosibirsk, 630090 Russia*
e-mail: m.k.baev@gmail.com, chernykh@ict.nsc.ru

Received February 1, 2011

Abstract—A closure of the Corrsin equation is performed using the gradient hypothesis connecting a third-order mixed correlation moment with a second-order two-point correlation function of a passive scalar field. A numerical model of the locally isotropic turbulence is constructed based on the closed system of the Kolmogorov and Yaglom equations. On the assumption of constant Loitsiansky and Corrsin invariants, a self-similar solution of the Corrsin equation is constructed corresponding to infinitely large Reynolds and Peclet numbers. A numerical model of the turbulence dynamics and temperature fluctuations behind a heated grid in a wind tunnel is constructed based on the closed Karman–Howarth and Corrsin equations.

Keywords: locally isotropic and isotropic turbulence, Karman–Howarth and Corrsin equations, Kolmogorov and Yaglom equations, numerical modeling.

DOI: 10.1134/S2070048212030027

INTRODUCTION

The dynamics of isotropic turbulence has attracted the attention of researchers for over 70 years. Many papers are devoted to theoretical and experimental studies of this problem [1]. In what follows, a brief analysis is presented of the results obtained using the Karman–Howarth and Corrsin equations [1]. Initially, the equations are not closed. Each equation contains two unknown functions. Consequently, the solution of these equations requires some additional information or hypotheses.

The main emphasis was placed on the closure of the Karman–Howarth equation. K. Hasselmann [2] was the first to suggest a connection between the correlation functions of the second and third orders. His model of the isotropic turbulence contains only one empirical constant and a rather complicated expression for the turbulent viscosity coefficient. Hasselmann did not use his model for any numerical calculations. Some calculation results obtained by its application are presented in V. Kostomakha's publications [3, 4]. In [3, 4] the most complete experimental data were obtained known to the authors about the decay of the longitudinal two-point correlation functions of the second and third order in a turbulent flow behind a non-heated grid. These experiments attained a high isotropy of the flow by its contraction; a detailed experimental verification was performed of the validity of the unclosed Karman–Howarth equation. The results are also presented for the comparison of the obtained experimental data with the authors' calculation using different other models of the isotropic turbulence decay.

M. Millionshchikov [5] proposed a different method for the closure of the Karman–Howarth equation. The coefficient of turbulent viscosity in his model was, however, such that the model yielded incorrect behavior of the solution for small values of the spatial variable. In order to address this defect, Millionshchikov introduced an additional empirical relationship between the spatial and time variables [6].

An original method of closure, free from the above-mentioned disadvantages, was proposed by Yu.M. Lytkin [7, 8]. Numerical experiments based on it and carried out in [8] demonstrated good agreement with the experimental data [9, 10]. Further, this model will be formulated in greater detail. Yet another method for the closure of the Karman–Howarth equation at high Reynolds numbers was implemented by J. Domaradzki and G. Mellor [11]. Their semiempirical model has the same drawback as Millionshchikov's model yielding an incorrect description of the solution behavior when the spatial variable is close to zero.

N. Akatnov [12, 13] proposed a closure using a complex representation of the coefficient of the turbulent viscosity and some empirical functions.

In 1993, M. Oberlack and N. Peters [14] published their work, in which the closure of the Karman–Howarth equation was implemented by the method similar to that suggested by Lytkin [7, 8]. They presented a comparison with the experimental data from the work by R.W. Stewart and A.A. Townsend [10] for the triple correlation function of the velocity field.

A. Onufriev [15] constructed a closed mathematical model for the dynamics of the isotropic turbulence based on a system of two differential equations for the double and triple longitudinal two-point correlation functions. He used a finite-dimensional equation for the probability density and Millionshchikov's approach (see, for instance, [1]) for the system closure. A. Onufriev showed that the model [7, 8] resulted from the truncation of the differential transport equations for the triple longitudinal correlation function of the velocity field.

G. Chernykh, Zh. Korobitsyna, and V. Kostomakha [16] numerically modeled the isotropic turbulence under its decay in the conditions of laboratory measurements [3, 4, 10, 17] based on the closed [7, 8] Karman–Howarth equation for the two-point correlation function of the velocity field. The Loitsiansky–Millionshchikov asymptotic solution [18, 19] was numerically implemented, which corresponded to the final stage of the decay.

Currently, investigations into the dynamics of the isotropic turbulence using the Karman–Howarth equation are continued. A.T. Onufriev and O.A. Pyrkova [20], and A.A. Onufriev, A.T. Onufriev, and O.A. Pyrkova [21] constructed a mathematical model for the decay of weak turbulence in a homogeneous isotropic turbulent flow taking into account the phenomenon of intermittency. The model is based on the closure of the Karman–Howarth equation and employs the gradient hypothesis connecting second- and third-order two-point correlation functions, and takes the dependence of the turbulent viscosity coefficient of the turbulent Reynolds number into account [15]. In the area of large turbulent Reynolds numbers, the expression for the turbulent viscosity coefficient in the model [20, 21] is consistent with that presented in [7, 8]. The obtained dependences for the scale of the fluctuating velocity and the longitudinal correlation function are consistent with the known asymptotic representations of the experimental data and the decay of the strong and weak isotropic turbulence. V. Frost studied the decay of the isotropic turbulence using Hasselmann's model [22]. The geometrical interpretation of the self-similar solution of the closed Karman–Howarth equation corresponding to the developed turbulence was carried out by V. Grebenev and M. Oberlack [23].

In addition to models based on the solution of the Karman–Howarth equation, there are also some other approaches to the theoretical study of the dynamics of the isotropic turbulence, among which we can name the analysis of the possible self-similar solutions of the unclosed Karman–Howarth equation or its spectral analysis, attempts to close the equation using the energy spectrum, direct numerical modeling of the isotropic turbulence based on the solution of Navier—Stokes equation, and the large-eddy method. These approaches and the obtained results were analyzed by G. Barenblatt and A. Gavrilov [24], A. Monin [1], A. Korneev, and L. Sedov [25]; U. Shumann and J. Patterson [26]; W. George [27], C. Speziale, and P. Bernard [28]; J. Chasnov [29], N. Mansour, and A. Wray [30]; O. Metais and M. Lesieur [31]; and others.

The dynamics of turbulent temperature fluctuations (passive scalar concentration) was considered in much fewer works (see, for example, [1, 32–35]). It is known [1] that the turbulence behind a grid in a wind tunnel is near-isotropic. In [35], as in [33], the main grid creating a near-isotropic turbulence was not heated. The heat supply was provided by a wire screen heated by an electric current placed in the flow behind the grid (in its immediate vicinity). The most complete (to the best of our knowledge) are the data of experiments carried out by R. Mills, A. Kistler, V. O'Brien, and S. Corrsin [33], in which measurements were made of near-isotropic pulsation characteristics of velocity and temperature fields depending on the distance from the grid. In particular, in [33], detailed data are presented about the dynamics of the second-order two-point correlation functions.

In a number of the works, the apparatus of the two-point correlation functions of the velocity fields and passive scalar is applied to the investigations of flows more complicated than isotropic turbulence (see, for example, [14, 36–40]).

As far as we are aware, the analysis of publications devoted to the study of a turbulent flow behind a heated grid enables us to conclude that the numerical modeling of the flow based on the closed system of Karman–Howarth and Corrsin equations [1, 32] is insufficiently studied. In this work, we performed the closure of the Corrsin equation by using the gradient hypothesis similar to the one proposed in [7, 8]. A numerical model of the locally isotropic turbulence has been constructed based on a closed system of Kolmogorov and Yaglom equations. In the assumption of constant Loitsiansky and Corrsin invariants [1, 19, 32], we obtained a self-similar solution of the Corrsin equation corresponding to infinitely large turbulent Rey-

nolds and Peclet numbers [1]. A numerical model of a turbulent flow behind a heated grid is constructed based on a system of closed Karman–Howarth and Corrsin equations. The calculation results have been compared with the experimental data [33]. This work is a development and continuation of [7, 8, 41, 42].

CLOSURE OF THE CORRSIN EQUATION

It is known that an isotropic turbulent flow and the dynamics of temperature fluctuations in it are described by a system of Karman–Howarth and Corrsin equations for two-point correlation functions of the velocity and temperature fields (the passive scalar) [1, 32]:

$$\frac{\partial B_{LL}}{\partial t} = \frac{1}{r^4}\frac{\partial}{\partial r} r^4 \left(B_{LL,L} + 2\nu \frac{\partial B_{LL}}{\partial r} \right); \tag{1}$$

$$\frac{\partial B_{\theta\theta}}{\partial t} = \frac{2}{r^2}\frac{\partial}{\partial r} r^2 \left(B_{L\theta,\theta} + \chi \frac{\partial B_{\theta\theta}}{\partial r} \right). \tag{2}$$

Here, B_{LL}, $B_{LL,L}$ are the second- and third-order longitudinal two-point correlation functions of the velocity field; $B_{\theta\theta}$ is the two-point correlation function of the temperature field; $B_{L\theta,\theta}$ is the mixed moment of the third order; ν and χ are the coefficients of kinematic viscosity and temperature conductivity (diffusion of the passive scalar).

Following [1], we obtain the integral scales of turbulence L_u, L_θ, and turbulent Reynolds and Peclet numbers from the relations $L_u = \frac{1}{u^2}\int_0^\infty B_{LL} dr$, $L_\theta = \frac{1}{\theta^2}\int_0^\infty B_{\theta\theta} dr$, $\mathrm{Re}_L = uL/\nu$, $\mathrm{Pe}_L = uL/\chi$, and $L = \min(L_u, L_\theta)$, where $u^2 = B_{LL}(0,t)$ and $\theta^2 = B_{\theta\theta}(0,t)$.

If the numbers Re_L and Pe_L are sufficiently large, then, as is known [1], there exists an equilibrium range of values $r \ll L$, over which (1) and (2) are reduced to equations for the structure functions D_{LL}, $D_{LL,L}$, $D_{\theta\theta}$, and $D_{L\theta,\theta}$ connected with B_{LL}, $B_{LL,L}$, $B_{\theta\theta}$, and $B_{L\theta,\theta}$ as follows:

$$D_{LL} = 2[u^2 - B_{LL}(r,t)], \quad D_{LL,L} = 6B_{LL,L}(r,t), \quad D_{\theta\theta} = 2[\theta^2 - B_{\theta\theta}(r,t)], \quad D_{L\theta,\theta} = 4B_{L\theta,\theta}(r,t).$$

The time dependence in these relations can be neglected and the consequences of Eqs. (1) and (2) have form [1]

$$D_{LL,L}(r) - 6\nu \frac{dD_{LL}(r)}{dr} = -\frac{4}{5}\varepsilon r; \tag{3}$$

$$D_{L\theta,\theta}(r) - 2\chi \frac{dD_{\theta\theta}(r)}{dr} = -\frac{4}{3} N r, \tag{4}$$

where $\varepsilon = -(3/2)\, du^2/dt$ and $N = -(1/2)\, d\theta^2/dt$ are the rates of the dissipation and equalization of temperature inhomogeneities (concentration inhomogeneities of the passive scalar), respectively. Equation (3) was derived by A.N. Kolmogorov [43]; equation (4) was obtained by A.M. Yaglom [44] (as a direct consequence of the Navier-Stokes equations).

Following [7, 8, 41], we express $B_{LL,L}$ and $B_{L\theta,\theta}$ in terms of B_{LL} and $B_{\theta\theta}$, using the relations of the gradient type

$$B_{LL,L} = 2K_1 \frac{dB_{LL}}{dr}, \quad B_{L\theta,\theta} = K_2 \frac{dB_{\theta\theta}}{dr},$$

or for the structure functions

$$-D_{LL,L} = 6K_1 \frac{dD_{LL}}{dr}, \quad -D_{L\theta,\theta} = 2K_2 \frac{dD_{\theta\theta}}{dr}, \tag{5}$$

Here, K_1 and K_2 are the coefficients of the turbulent viscosity and diffusion. We find K_1 and K_2 in the following way [7, 41]:

$$K_1 = æ_1 r\sqrt{D_{LL}}, \quad K_2 = æ_2 r\sqrt{D_{LL}}. \tag{6}$$

where $æ_1$ and $æ_2$ are empirical constants. Taking into account (5), the system of equations (3), (4) can be written as

$$(K_1 + \nu)\frac{dD_{LL}}{dr} = \frac{2}{15}\varepsilon r; \tag{7}$$

$$(K_2 + \chi)\frac{dD_{\theta\theta}}{dr} = \frac{2}{3}Nr. \tag{8}$$

The initial conditions for system (7) and (8) are

$$D_{LL} = D_{\theta\theta} = 0, \quad r = 0. \tag{9}$$

From the solution of equations (7) and (8), it follows [1] that in the inertial-convective range $L \gg r \gg \eta$, $\eta = \max(\eta_u, \eta_\theta)$, $\eta_u = (\nu^3/\varepsilon)^{1/4}$, and $\eta_\theta = (\chi^3/\varepsilon)^{1/4}$, over which $K_1 \gg \nu$, $K_2 \gg \chi$ and the quantities D_{LL} and $D_{\theta\theta}$ are equal respectively to

$$D_{LL} = (1/5æ_1)^{2/3}(\varepsilon r)^{2/3} = C_u(\varepsilon r)^{2/3}, \tag{10}$$

$$D_{\theta\theta} = \left(1/æ_2\sqrt{C_u}\right)N\varepsilon^{-1/3}r^{2/3} = C_\theta N\varepsilon^{-1/3}r^{2/3}.$$

In these equations expressing the law of two-thirds, the values C_u and C_θ are universal constants. In [1], the value $C_u = 1.9$ is suggested based on the processing of a large number of experimental data; hence, in [7] it was obtained that $æ_1 = 0.076$. The value recommended in [1] is $C_\theta = 3.0$; it corresponds to $æ_2 = 0.242$.

From the structure functions D_{LL} and $D_{\theta\theta}$ found by solving the problem (7)–(9) of one-dimensional spectra of velocity fields and the passive scalar (k is the wave number), can be calculated [1]

$$E_{1u} = \frac{1}{\pi k}\int_0^\infty \frac{dD_{LL}}{dr}\sin krdr,$$

$$E_{1\theta} = \frac{1}{\pi k}\int_0^\infty \frac{dD_{\theta\theta}}{dr}\sin krdr. \tag{11}$$

For calculations and comparison with experimental data [3, 4, 45–48], the dimensionless system of equations (7) and (8)was written as follows:

$$\frac{dD^*_{LL}}{dr^*} = \frac{(2/15)r^*}{1 + æ_1 r^*\sqrt{D^*_{LL}}}; \tag{12}$$

$$\frac{dD^*_{\theta\theta}}{dr^*} = \frac{(2/3)\,\mathrm{Pr}\, r^*}{1 + æ_2\,\mathrm{Pr}\, r^*\sqrt{D^*_{LL}}}. \tag{13}$$

Here, $r^* = r/\eta_u$, $D^*_{LL} = D_{LL}/v_\eta^2$, $D^*_{\theta\theta} = D_{\theta\theta}/\theta_k^2$, $\mathrm{Pr} = \nu/\chi$, $v_\eta = (\nu\varepsilon)^{1/4}$, and $\theta_k = (N\eta_u/v_\eta)^{1/2}$.

The Cauchy problem (7)–(9) was solved using the standard Runge-Kutta method of the fourth-order accuracy [49]. Moreover, the solution was found at the grid nodes $r_i = r_{i-1} + h_i$, $i = 1,..., I$; $r_0 = 0$. A rather high value of r_I was selected. In order to calculate one-dimensional spectra (11) using the values $f_{1i} = \left(\frac{dD_{LL}}{dr}\right)_i$, $f_{2i} = \left(\frac{dD_{\theta\theta}}{dr}\right)_i$ found in (7) and (8), cubic interpolating splines were constructed and Filon's method was applied [50]. The algorithm for spectra calculation was tested by computing the Fourier transforms of the functions e^{-x}, e^{-x^2}, $\frac{x}{\beta^2 + x^2}$, and $\beta = \mathrm{const}$. The exact analytical values of these quantities are known. The values of the wave number varied so that the Fourier cosine transform decreased by 15, 15, and 11 orders, respectively. The calculated values of the Fourier transforms coincide with their analytical values with an accuracy of up to 3–4 significant digits. As an example, Table 1 shows the calculation results for a cosine Fourier transform of the function e^{-x^2}. Column 1 presents the exact analytical values $\int_0^\infty e^{-x^2}\cos kxdx$; column 2 shows the results of calculations performed in the present work using the above-described technique; in column 3 the results of the calculations are given obtained by a standard *Filoth*

Table 1. Comparison of the calculated and exact values of the Fourier cosine transform

k	I	II	III
1	6.9019422352E-01	6.9019422352E-01	6.9019408793E-01
5	1.7108204339E-03	1.7108204340E-03	1.7108073053E-03
10	1.2307869792E-11	1.2307473130E-11	1.2307775326E-11
11	6.4585773190E-14	6.4432149597E-14	6.4585056752E-14
11.5	3.8786771597E-15	3.8828485725E-15	3.8786303172E-15
12	2.0556235864E-16	2.0511051610E-16	2.0554924279E-16
12.5	9.6142794521E-18	6.9354614471E-18	9.6164072352E-18

program [51]. The results of column 2 were obtained using an irregular grid ($h_i = h_{i-1} \times 1.0025$) with the node number 5000, initial step $h_1 = 0.0000001$ and $r_I = 10$. It can be seen that that the standard *Filoth* program allows calculations for large values of wave number k, but it requires an analytical definition of the function. Varying the number of grid points and the values of the initial step does not lead to any significant deviations.

In our work, along with model (12) and (13), we also considered the closure of the system of equations (3) and (4) based on A.M. Obukhov's model [1]

$$D_{LL,L} = -|S|(D_{LL})^{1/2}, \quad D_{L\theta,\theta} = -|F| D_{LL}^{1/2} D_{\theta\theta}, \tag{14}$$

where $S = -0.306$ and $F = -0.322$ are the empirical constants. The closed system of equations in this case can be written as

$$\frac{dD_{LL}^*}{dr^*} = -\frac{|S|}{6}\left(D_{LL}^*\right)^{2/3} + \frac{2}{15}r^*, \tag{15}$$

$$\frac{1}{\mathrm{Pr}}\frac{dD_{\theta\theta}^*}{dr^*} = -\frac{|F|}{2}\left(D_{LL}^*\right)^{1/2} D_{\theta\theta}^* + \frac{2}{3}r^*. \tag{16}$$

The initial conditions for D_{LL} and $D_{\theta\theta}$ remain zero. System (15) and (16) was numerically integrated both by an implicit refined Euler–Cauchy method [49] and using the standard Runge-Kutta method of the fourth-order accuracy. When the latter method was applied, for reasons of stability the calculations were performed on the interval $0 \le r^* \le R_0^*$ (in the calculations it was assumed $R_0^* = 200$), which was later followed by the transition to asymptotic representations (10). A similar approach was also used for the numerical integration of the system of equations (12) and (13), along with direct numerical integration (in order to control the accuracy of the calculations).

The results of the calculations based on model (12) and (13) were compared with the experimental data [45, 46] (Figs. 1, 2; Pr = 0.72). In Fig.1a, the calculated longitudinal structure functions of the velocity fields and the passive scalar (temperature) of the second order are compared with the experimental data [45]. The agreement appears to be satisfactory. The structure functions of the third order, calculated using model (12) and (13) are compared with the experimental data [45] shown in Fig.1b; the agreement is sufficiently good. Good agreement was also obtained for the results of measurements of the two-point longitudinal structure functions of the velocity field of the second and third orders [3, 4].

In addition, in Fig. 2, the calculated second-order structure function of the temperature field is compared with the experimental data [46]. The scatter of the experimental data is rather large.

The one-dimensional spectrum of the velocity field calculated from the solution of Eq. (12) is compared in Fig. 3 with the measurement results in various turbulent flows collected in [47] (comparisons with earlier studies, available at the time of performance, are presented in [3, 4, 7]). It is obvious that there is good agreement with the experimental data. This figure also shows the results of the calculations using model (15). Obukhov's model gives a somewhat more rapid decrease in the one-dimensional spectrum, which is consistent with the results obtained in Golitsyn's study [52].

The calculated one-dimensional spectrum of the passive scalar field is compared with the results of the measurements presented in [48] and known asymptotics [1] in Fig. 4. The agreement is satisfactory. We note that by the authors' estimates [48], the value $C_\theta \approx 2.8$. In the present work, following recommenda-

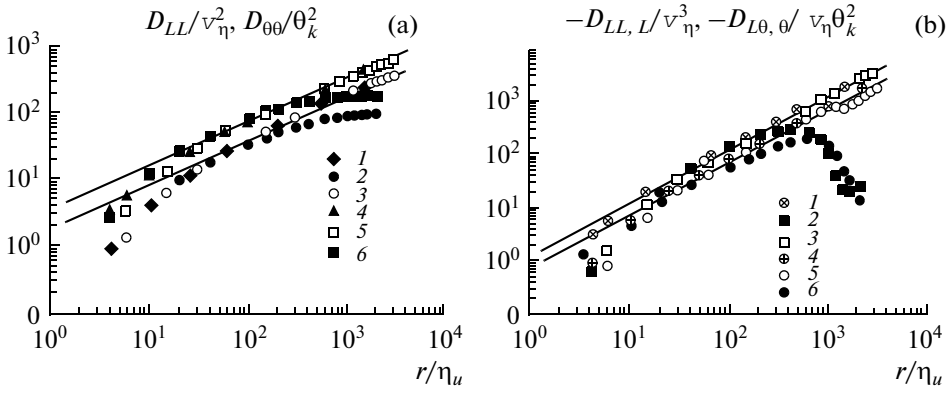

Fig. 1. Changes depending on r/η_u in the calculated and measured [45] structure functions of the velocity and temperature fields: (a) the calculated longitudinal structure function of the velocity field D_{LL} (point *1*) and structure function of the temperature field $D_{\theta\theta}$ (point *4*); points *2*, *3* are results of D_{LL} measurements; points *5* and *6* are the results of the $D_{\theta\theta}$ measurements; (b) the calculated structure functions $D_{LL,L}$ and $D_{L\theta,\theta}$ (points *1* and *4*); points *2* and *3* are the results of $D_{LL,L}$ measurements; points *5* and *6* are the results of $D_{L\theta,\theta}$ measurements. Points *3* and *5* in Figs. 1a and 1b correspond to $\mathrm{Re}_\lambda = 7200$; points *4* and *6* correspond to $\mathrm{Re}_\lambda = 250$.

tions [1], $C_\theta = 3$ was chosen. Batchelor's theory [1] corresponding to $\mathrm{Pr} \gg 1$ also comprises an empirical constant matched in [48] during the comparison with the experimental data (Fig. 4) to $C_\theta = 2.8$.

Note that the validity of the approximation of local isotropy with respect to the field of the passive scalar [53] has often been discussed in many publications. In our view, the above-presented comparison of the calculation results and experimental data is, to some extent, a positive answer to this question.

Following [1, 43, 44], we note some solution properties of the Cauchy problem (7)–(9). First of all, under $r \ll \eta_u$ ($r^* \ll 1$), we have $D_{LL}^* \approx (r^*)^2/15$, and $D_{\theta\theta}^* \approx (\mathrm{Pr}/3)(r^*)^2$. These asymptotics are obtained in the above-cited works from the analysis of the solution of the Cauchy problem for a nonclosed system of equations (3) and (4) under the assumption that the third-order moments are small. On the assumption $\mathrm{Pr} \gg 1$ and of the validity of the above-mentioned asymptotic representation $D_{LL}^* \approx (r^*)^2/15$, there exists a range of values $(\mathrm{Pr})^{-1/2} \ll r^* \ll 1$, in which $D_{\theta\theta}^* \approx (\sqrt{15}/3\text{æ}_2)\ln(\text{æ}_2(r^*)^2/\sqrt{15})$. The latter [1] corresponds to the representation $E_{1\theta} \sim k^{-1}$ on some interval of wave numbers (see Fig. 4).

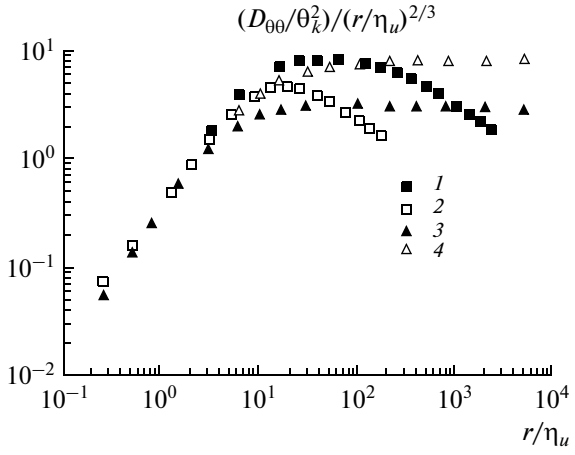

Fig. 2. Calculated and measured second-order structure functions of the temperature field: Points *1* and *2* are experimental data [46], $\mathrm{Re}_\lambda = 230$; 40; points *3* and *4* are the calculation results corresponding to $\text{æ}_2 = 0.242$; 0.095.

In the conclusion of this section, we also note that representation (6) of the coefficients of the turbulent viscosity and diffusion makes it possible to close the system of equations (1) and (2) and to calculate the correlation functions B_{LL} and $B_{\theta\theta}$ not only in the equilibrium range but also for all values of r. The self-similar solution of the closed system of Eqs. (1) and (2), corresponding to $\nu = \chi = 0$, under the assumption of the constancy of the Loitsiansky and Corrsin invariants [1, 19, 32, 33] and the fulfillment of the boundary conditions

$$B_{LL,L} = 2K_1\frac{\partial B_{LL}}{\partial r} = B_{L\theta,\theta} = K_2\frac{\partial B_{\theta\theta}}{\partial r} = 0, \quad r = 0;$$
$$B_{LL} = B_{\theta\theta} \to 0, \quad r \to \infty,$$

has the form

$$B_{LL} = u^2 f(r/L) = u^2 f(\xi), \quad B_{\theta\theta} = \theta^2\varphi(\xi), \quad \xi = r/L, \quad (17)$$

$$-2\sqrt{1-f} + \ln(1+\sqrt{1-f}) - \ln(1-\sqrt{1-f}) = (2/3)\xi, \quad (18)$$

$$u = A(t-t_0)^{-5/7}, \quad L = (14\sqrt{2}/3)\text{æ}_1 A(t-t_0)^{2/7}, \quad (19)$$

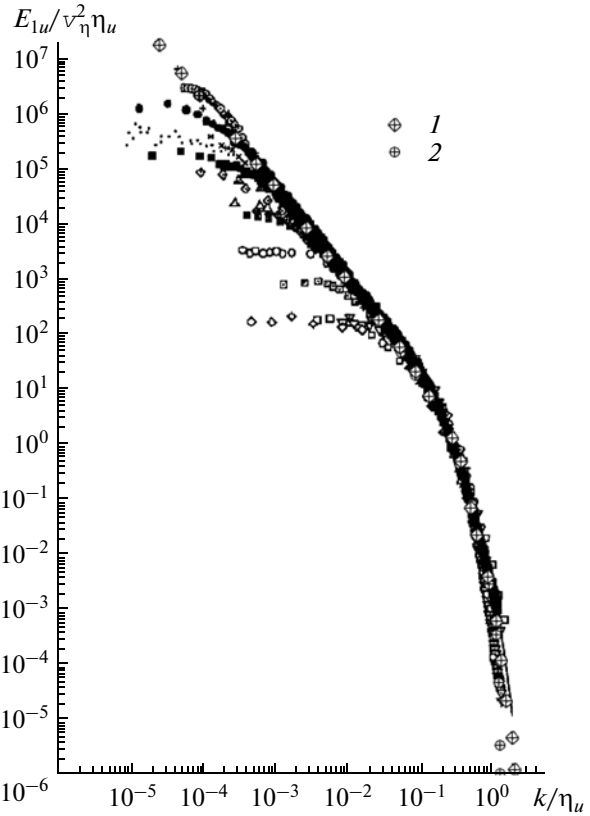

Fig. 3. Comparison of the calculated one-dimensional spectrum of the velocity field (points *1*, *2*) with the experimental data collected in [47]; points *1* and *2* are calculation results (point *1* is obtained by using model (12); point *2*, by using model (15)).

$$\varphi = \exp[-(2\text{æ}_1/3\text{æ}_2)\int_0^\xi (1/\sqrt{1-f})d\xi]; \quad \theta^2 = K/L^3Q_\theta. \tag{20}$$

Here, $A^7 = \Lambda/\left(Q_u\left(14\text{æ}_1\sqrt{2}/3\right)^5\right)$, $\Lambda(t) = \int_0^\infty r^4 B_{LL}(r,t)dr$, $K(t) = \int_0^\infty r^2 B_{\theta\theta}(r,t)dr$ are the Loitsiansky and Corrsin invariants; $t_0 = \text{const}$; and $Q_u = \int_0^\infty \xi^4 f(\xi)d\xi$, $Q_\theta = \int_0^\infty \xi^2\varphi(\xi)d\xi$. Note that it follows from (20) that $\varphi \approx 1 - (2\text{æ}_1/3\text{æ}_2)\xi^{2/3} = \varphi_0(\xi)$ at small ξ. The self-similar solution (18), (19) was obtained by Lytkin in [7]. The laws of decay of (19) are consistent with the known laws of Kolmogorov [1, 43]. The plotted function $\varphi(\xi)$ is presented in Fig. 5. Along with $\varphi(\xi)$, Fig. 5 also shows the function $\varphi_1(\xi) = \exp(-(2\text{æ}_1/3\text{æ}_2)\xi)$, i.e., the self-similar solution of the Corrsin equation closed with the help of the simplified Millionshchikov model [5, 6], in which it was assumed $K_1 = \text{æ}_1 r\sqrt{B_{LL}(0,t)}$ and $K_2 = \text{æ}_2 r\sqrt{B_{LL}(0,t)}$. The law of the θ^2 decay seems to have first been presented by Corrsin [32].

A detailed discussion of the constancy of the Loitsiansky and Corrsin invariants can be found in a number of works [1, 8, 16, 19, 29, 54–59]. In [8, 16, 57], the constancy of the Loitsiansky invariant follows from the assigned initial conditions consistent with the experimental data and the applied numerical model.

NUMERICAL MODELING OF A TURBULENT FLOW BEHIND A HEATED GRID IN A WIND TUNNEL

As noted in the introduction, near-isotropic turbulence can be generated in the laboratory conditions by placing a swirling grid in the test section of a wind tunnel or a flow channel. The results of the measurements of correlation functions in the flow behind the swirling grids can be used for comparison with the

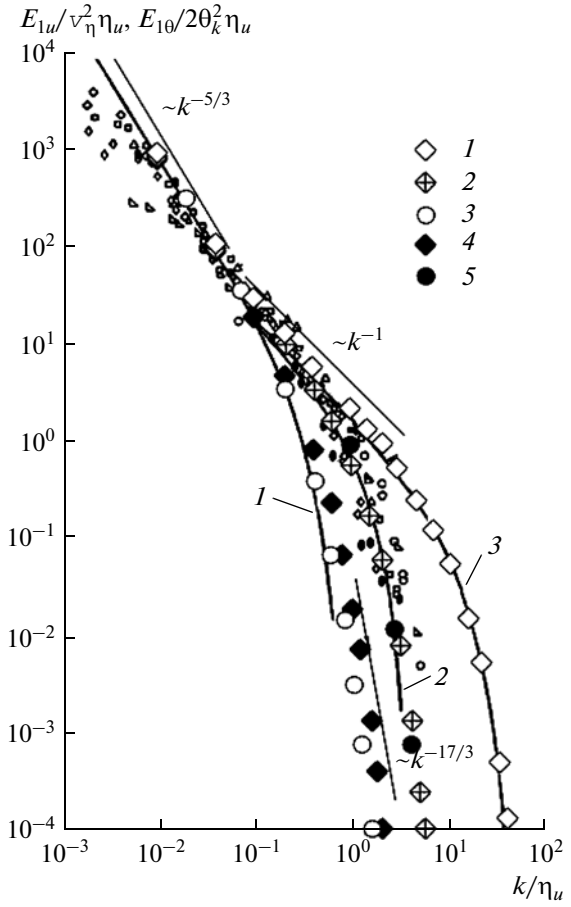

Fig. 4. Comparison of calculated and measured [48] one-dimensional spectra of the fields of velocity and the passive scalar; Points *1*, *2*, and *3* correspond to $E_{1\theta}$ for Pr = 700; 7; and 0.72; *4* is the calculated spectrum E_{1u}; *5* are the calculations using the Obukhov model, Pr = 7; Curve *1* is processing [48] of the experimental data of a one-dimensional spectrum of the velocity field; curves *2* and *3* are theoretical Batchelor curves for a one-dimension spectrum of the passive scalar, Pr = 7; 700; small-size signs are experimental data [48].

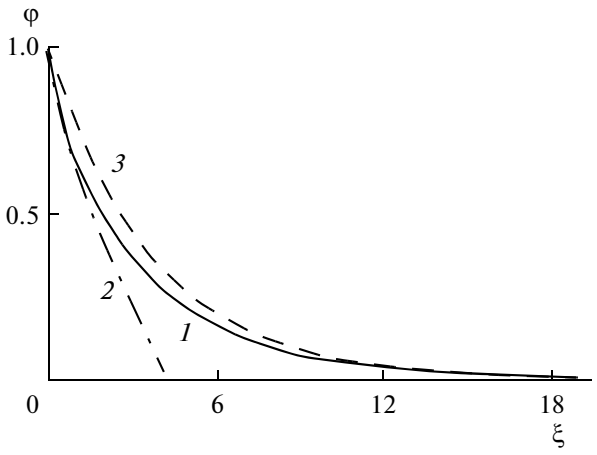

Fig. 5. The self-similar solution of the Corrsin equation corresponding to $Q_u = 100$; (*1*) $\varphi(\xi)$ is determined by formula (20); (*2*) function $\varphi_0(\xi) = 1 - (2æ_1/3æ_2)\xi^{2/3}$; (*3*) function $\varphi_1(\xi) = \exp(-(2æ_1/3æ_2)\xi)$.

calculation results. It is convenient at the same time to write the closed equations (1) and (2) in a dimensionless form as follows:

$$\frac{\partial \tilde{B}_{LL}}{\partial \tilde{t}} = \frac{2}{\tilde{r}^4}\frac{\partial}{\partial \tilde{r}}\tilde{r}^4\left(\tilde{K}_1 + \frac{1}{\mathrm{Re_M}}\right)\frac{\partial \tilde{B}_{LL}}{\partial \tilde{r}}; \qquad (21)$$

$$\frac{\partial \tilde{B}_{\theta\theta}}{\partial \tilde{t}} = \frac{2}{\tilde{r}^2}\frac{\partial}{\partial \tilde{r}}\tilde{r}^2\left(\tilde{K}_2 + \frac{1}{\mathrm{Pe_M}}\right)\frac{\partial \tilde{B}_{\theta\theta}}{\partial \tilde{r}}. \qquad (22)$$

Here, $\tilde{B}_{LL} = B_{LL}/U_\infty^2$; $\tilde{t} = x/M$; $\tilde{r} = r/M$; $\tilde{K}_1 = K_1/(MU_\infty)$; $\mathrm{Re_M} = U_\infty M/\nu$; $\tilde{B}_{\theta\theta} = B_{\theta\theta}/\Theta^2$; $\tilde{K}_2 = K_2/(MU)_\infty$; $\mathrm{Pe_M} = U_\infty M/\chi = \mathrm{Re_M Pr}$; x is the distance from the grid; U_∞, Θ is the flow velocity and temperature in the test section of the wind tunnel or the channel; M is the cell size of the swirling grid; and Re_M, Pe_M are the Reynolds and Peclet numbers.

We supplement the system of equations (21) and (22) with the boundary conditions

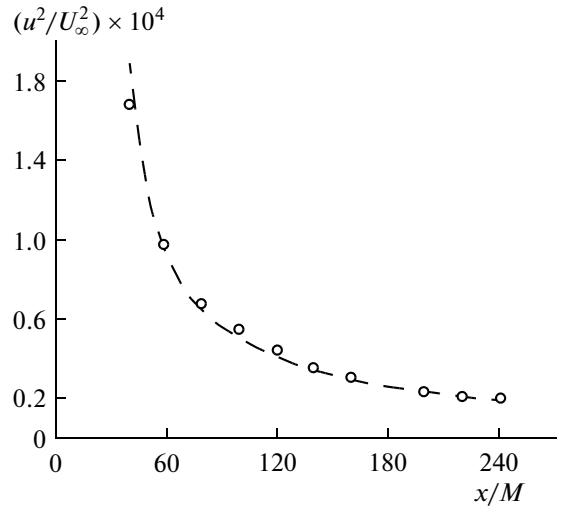

Fig. 6. Dependence of the value $u^2 = B_{LL}(0, t)$ on the distance from the grid: points are the experimental data; line is the calculation results.

$$\tilde{r} = 0: \ \frac{\partial \tilde{B}_{LL}}{\partial \tilde{r}} = \frac{\partial \tilde{B}_{\theta\theta}}{\partial \tilde{r}} = 0; \qquad \tilde{r} \to \infty: \ \tilde{B}_{LL} \to 0, \ \tilde{B}_{\theta\theta} \to 0 \tag{23}$$

and the initial conditions

$$\tilde{B}_{LL}(\tilde{r}, \tilde{t}_0) = \phi_1(\tilde{r}), \quad \tilde{B}_{\theta\theta}(\tilde{r}, \tilde{t}_0) = \phi_2(\tilde{r}). \tag{24}$$

In accordance with the physical meaning of the problem, functions $\phi_1(\tilde{r})$, $\phi_2(\tilde{r})$ must be continuous, bounded, have a maximum at $\tilde{r} = 0$, and tend to zero under $\tilde{r} \to \infty$.

Under the assumption of a sufficiently rapid decay of functions $\phi_1(\tilde{r})$, $\phi_2(\tilde{r})$ and the solution $\tilde{B}_{LL}$, $\tilde{B}_{\theta\theta}$ of problem (21)–(24) under $\tilde{r} \to \infty$, the consequence of Eqs. (21) and (22) is the known Loitsiansky and Corrsin invariants [1, 19, 32, 33]

$$\int_0^\infty \tilde{B}_{LL}\tilde{r}^4 d\tilde{r} = \tilde{\Lambda}(\tilde{t}) = \text{const} = \tilde{\Lambda}(\tilde{t}_0), \qquad \int_0^\infty \tilde{B}_{\theta\theta}\tilde{r}^2 d\tilde{r} = \tilde{K}(\tilde{t}) = \text{const} = \tilde{K}(\tilde{t}_0).$$

In the following, the nondimensionalization sign "~" is omitted.

For the numerical solution of (21)–(24), implicit conservative difference schemes were used based on the integro-interpolation method [60]

$$\frac{(B_{LL})_i^{n+1,s+1} - (B_{LL})_i^n}{\tau_n} = \frac{2}{r_i^4 \hbar_{i-1}}\left(P_{i+1/2}^{n+1,s} \frac{(B_{LL})_{i+1}^{n+1,s+1} - (B_{LL})_i^{n+1,s+1}}{h_i} - P_{i-1/2}^{n+1,s} \frac{(B_{LL})_i^{n+1,s+1} - (B_{LL})_{i-1}^{n+1,s+1}}{h_{i-1}} \right), \tag{25}$$

$$\frac{(B_{\theta\theta})_i^{n+1} - (B_{\theta\theta})_i^n}{\tau_n} = \frac{2}{r_i^2 \hbar_{i-1}}\left(H_{i+1/2}^{n+1} \frac{(B_{\theta\theta})_{i+1}^{n+1} - (B_{\theta\theta})_i^{n+1}}{h_i} - H_{i-1/2}^{n+1} \frac{(B_{\theta\theta})_i^{n+1} - (B_{\theta\theta})_{i-1}^{n+1}}{h_{i-1}} \right). \tag{26}$$

Here, $P = r^4\left(\frac{1}{\mathrm{Re_M}} + K_1\right)$, $H = r^2\left(\frac{1}{\mathrm{Pe_M}} + K_2\right)$; n is the number of the time layer; τ_n and h_i ($n = 0, 1, ..., N$; $i = 0, 1, ..., I$) are the steps of the difference grid in the temporal and spatial variables, respectively; $\hbar_i = 0.5(h_i + h_{i+1})$, $r_i = r_{i-1} + h_i$, and s is the number of the iteration with respect to nonlinearity;

$$P_i^{n+1} = P(r_i, t_{n+1}), \quad H_i^{n+1} = H(r_i, t_{n+1}), \quad P_{i\pm1/2} = 0.5(P_i + P_{i\pm1}), \quad H_{i\pm1/2} = 0.5(H_i + H_{i\pm1}); \quad t_{n+1} = t_n + \tau_n.$$

In accordance with the boundary and initial conditions (23) and (24), the following initial-boundary conditions were set for solving the finite-difference problem

$$(B_{LL})_i^0 = \phi_1(r_i); \quad (B_{\theta\theta})_i^0 = \phi_2(r_i), \tag{27}$$

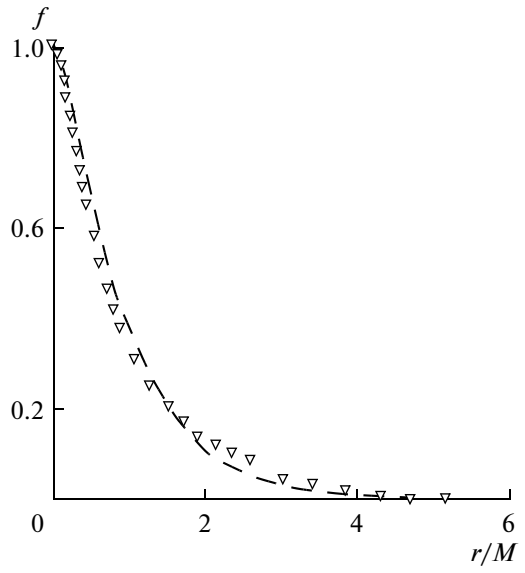

Fig. 7. Calculated and experimental normalized correlation functions $f(r) = B_{LL}(r, t)/B_{LL}(0, t)$ at $t = x/M = 200$: points are the experimental data; line is the calculation results.

$$(B_{LL})_0^{n+1,s+1} = (B_{LL})_1^{n+1,s+1};\ \ (B_{\theta\theta})_0^{n+1} = (B_{\theta\theta})_1^{n+1};$$
$$(B_{LL})_I^{n+1,s+1} = (B_{\theta\theta})_I^{n+1} = 0. \qquad (28)$$

A sufficiently large value r_I was selected. In performing iterations with respect to nonlinearity it was assumed that $(B_{LL})_i^{n+1,0} \equiv (B_{LL})_i^n$. Iterations with respect to nonlinearity were performed until the condition $\max_i \left|(B_{LL})_i^{n+1,s+1} - (B_{LL})_i^{n+1,s}\right| \le \delta \max_i (B_{LL})_i^{n+1,s}$ was fulfilled, where the value $\delta > 0$ was selected within the range $\delta = 10^{-5}$–10^{-4} (the further decrease in δ did not lead to any significant change in the solution). To achieve this accuracy, it was sufficient to make 3.5 iterations with respect to nonlinearity (Eq. (25)) at each time layer. Parameters τ_n, h_i I, and δ were chosen experimentally in the course of the calculations.

The numerical model was tested on the problem of the turbulence decay behind an unheated grid [3, 4]. The initial conditions at $t_0 = 40$ were established on the basis of the experimental data. The changes in the dependence of the calculated and measured values $B_{LL}(0, t)$ on the distance from the grid are presented in Fig. 6. The calculated normalized correlation function $f(r) = B_{LL}(r,t)/B_{LL}(0,t)$ for $t = 200$ is compared with the measured one in Fig. 7. It is obvious that the calculation results in Figs. 6 and 7 are in good agreement with the experimental data (earlier, a detailed comparison had been carried out in [3, 4, 16]).

The experiments [33] in a wind tunnel contained fairly detailed measurements of turbulence characteristics behind a heated grid at $\mathrm{Re_M} = 7200$ and $\mathrm{Pe_M} = 5184$. Under $t = x/M = 17.0$, the initial conditions were specified as the correlation functions B_{LL}/U_∞^2, $B_{\theta\theta}/\Theta^2$ obtained in [33]. Before proceeding to the comparison of the calculated correlation functions of the temperature and experimental data [33], it should be noted that the quantity $æ_2$ was assumed to be equal to 0.095 on the basis of the condition of its better agreement with the experimental data. Its value is consistent with our results shown in Fig. 2. The changes in the values $u/U_\infty = \sqrt{B_{LL}(0,t)}/U_\infty$ and $\theta = \sqrt{B_{\theta\theta}(0,t)}/\Theta$ with the increase in $t = x/M$ is presented in Fig. 8. It is evident that the calculation results are fairly close to the experimental data. At $æ_2 = 0.125$

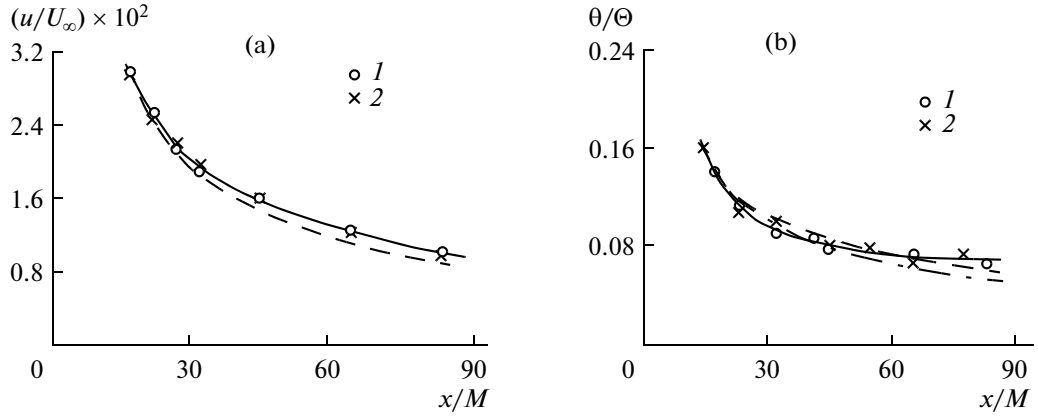

Fig. 8. Dependences of the quantities u/U_∞ (a) and θ/Θ (b) on the value x/M: *1* and *2* are experimental data [33] (for (a): (*1*) behind a heated grid; (*2*) behind a cold grid; (b) signs *1*, *2* correspond to different experiments); solid lines are the results of processing the experimental data in [33]; dashed lines are the calculation results under $æ_2 = 0.095$; the dashed-dotted line is the calculation results for $æ_2 = 0.125$.

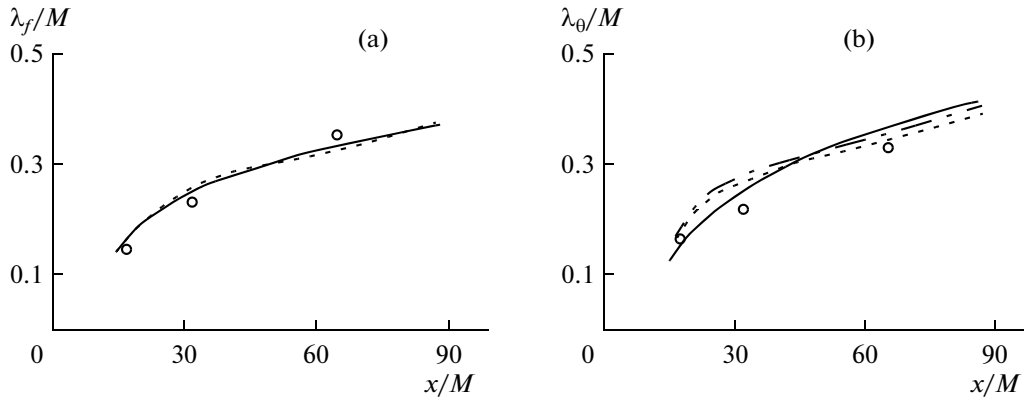

Fig. 9. Taylor λ_f (a) and Corrsin λ_θ (b) microscales: points are experimental values obtained in [33] (a – λ_{1f}; b – $\lambda_{1\theta}$); solid lines are results of processing of the experimental data in [33] (a – λ_{2f}; b – $\lambda_{2\theta}$); stroked, dashed, and dotted-dashed lines are results of the calculation made in the present work (a – λ_{1f}, λ_{2f}, λ_{3f}, respectively; b – $\lambda_{1\theta}$, $\lambda_{2\theta}$, $\lambda_{3\theta}$, respectively).

(which corresponds to the value $C_\theta = 5.8$ [1]), a greater deviation of the calculation results from the experimental data is observed.

As is known, the turbulent flow behind a heated grid is characterized by two microscales, i.e., λ_f and λ_θ [1, 32, 33]. Each of those can be found in two ways. By definition, Taylor λ_{1f} and Corrsin $\lambda_{1\theta}$ microscales are obtained from the relations [1, 32, 33]

$$\frac{1}{\lambda_{1f}^2} = -\frac{1}{2}\left(\frac{\partial^2 f}{\partial r^2}\right)\Bigg|_{r=0}, \quad \frac{1}{\lambda_{1\theta}^2} = -\frac{1}{2}\left(\frac{\partial^2 m}{\partial r^2}\right)\Bigg|_{r=0}, \quad m(r) = \frac{B_{\theta\theta}(r,t)}{B_{\theta\theta}(0,t)}. \tag{29}$$

In [33], the relations

$$\frac{du^2}{dt} = -20\frac{1}{\mathrm{Re_M}}\frac{u^2}{\lambda_{2f}^2}, \quad \frac{d\theta^2}{dt} = -12\frac{1}{\mathrm{Pe_M}}\frac{\theta^2}{\lambda_{2\theta}^2}. \tag{30}$$

resulting from the Taylor expansion of all terms of equations (1) and (2) are also employed. According to the terminology adopted in [1], these relations are zero terms of the expansion when $r = 0$. In [33], relations (29) and (30) are treated as independent and are used to control the accuracy of the measurements. It should be expected that the values λ_{1f} and λ_{2f} will be close. These values coincide only for parabolic correlation functions $f(r) = 1 - r^2/\lambda_f^2$ (for small r). The measurement results [33] are sufficiently close. The results of numerical simulations are practically the same. A similar situation with the experimental data is also observed for the values $\lambda_{1\theta}$ and $\lambda_{2\theta}$. The calculated values λ_{1f} and λ_{2f} differ but insignificantly.

It should be noted that the equalities $\lambda_{1f} = \lambda_{2f}$ and $\lambda_{1\theta} = \lambda_{2\theta}$ do not follow from the numerical model. The calculated microscale values result from the computer processing of the data obtained by a numerical experiment (in [33] by a laboratory experiment). In this paper, we consider also a modification of the numerical model, in which, under $r = 0$, boundary conditions were set for the correlation functions instead of the Neumann condition (23) (thereby introducing into the model the equality of the microscales obtained from relations (29) and (30)):

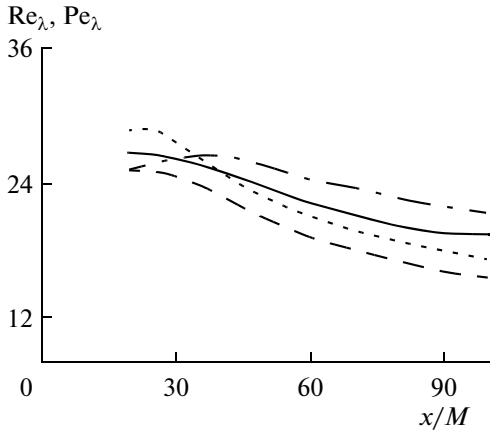

Fig. 10. Calculated and experimental values of the turbulent Reynolds and Peclet numbers. Solid line is the experimental data for Re_λ; stroked line is calculated value of Re_λ; dashed-dotted line is the experimental data for Pe_λ; and dashed line is the calculated values of Pe_λ.

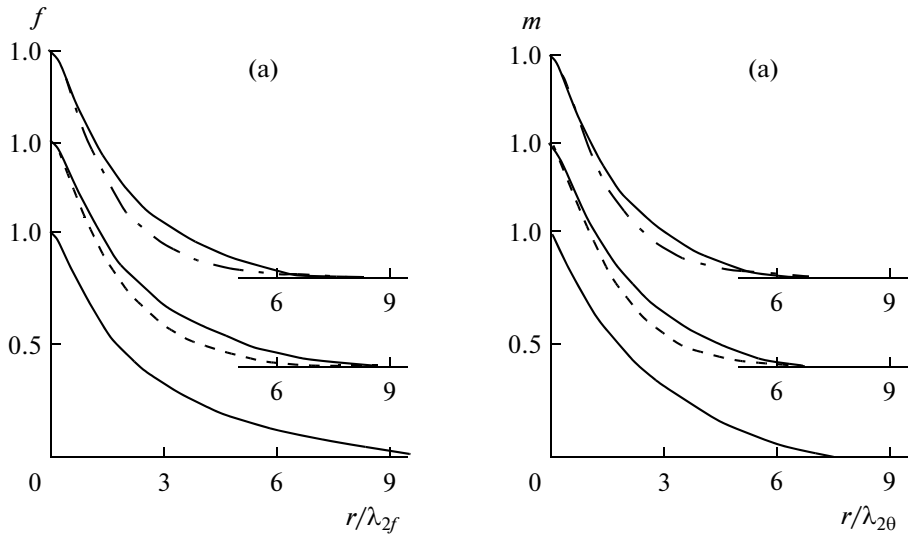

Fig. 11. Calculated and experimental normalized correlation functions: (a) $f(r) = B_{LL}(r,t)/B_{LL}(0,t)$; (b) $m(r) = B_{\theta\theta}(r,t)/B_{\theta\theta}(0,t)$; solid lines are experimental data; (*1*) $x/M = 17.0$; (*2*) $x/M = 32.0$; (*3*) $x/M = 65.0$; dashed lines are calculation results for $t = x/M = 32.0$; dashed-dotted lines are calculation results at $t = x/M = 65.0$.

$$\left(\frac{\partial B_{LL}}{\partial t}\right)\Big|_{r=0} = \frac{10}{\mathrm{Re}_M}\left(\frac{\partial^2 B_{LL}}{\partial r^2}\right)\Big|_{r=0}, \quad \left(\frac{\partial B_{\theta\theta}}{\partial t}\right)\Big|_{r=0} = \frac{6}{\mathrm{Pe}_M}\left(\frac{\partial^2 B_{\theta\theta}}{\partial r^2}\right)\Big|_{r=0}. \tag{31}$$

The values λ_{3f} and $\lambda_{3\theta}$ found are close to the values λ_{1f}, λ_{2f}, $\lambda_{1\theta}$, and $\lambda_{2\theta}$ (Fig. 9). The influence of the boundary conditions (31) on the calculated values of $B_{LL}(r, t)$ and $B_{\theta\theta}(r, t)$ proved to be negligible. The grid values of the correlation functions differ by no more than 1% in the uniform grid norm for all the considered range of t values.

The values of the turbulent Reynolds and Peclet numbers $\mathrm{Re}_\lambda = u\lambda_f/\nu$, $\mathrm{Pe}_\lambda = u\lambda_\theta/\chi$ were calculated from the values $u = \sqrt{B_{LL}(0,t)}$, λ_f, and λ_θ found in the numerical experiments. It was established that under $t = x/M = 20$–65, the values of the turbulent Reynolds and Peclet numbers decrease and are in the ranges $\mathrm{Re}_\lambda = 26.1$–$35.6$, $\mathrm{Re}_\lambda = 26.1$–$20.3$ (Fig. 10).

These data are consistent with the experimental data [33] indicating a weak variation of the turbulent Reynolds and Peclet numbers at the initial stage of the turbulence decay behind the grid. The slow change in Re_λ was mentioned, in particular, in [3, 4, 8, 16, 57]. Above, in formulating the closing relations (5) and (6), it has been noted that the empirical constant $æ_1$ calculated in terms of the universal Kolmogorov constant C_u, corresponding to the representation of the structure function D_{LL} within the inertial range of scales. The performed numerical experiments (see also [3, 4, 7, 8, 16, 57]) showed that the value $æ_1$ was sufficiently universal. As for the empirical constant $æ_2$, as has been noted above, the value $æ_2 = 0.095$ was chosen taking into account the compliance with the requirement of the agreement between the calculation results and the experimental data [33] (see also Fig. 2). The choice of $æ_2 = \mathrm{const}$ for the numerical simulation of the dynamics of turbulent fluctuations of temperature at the initial stage of modeling the decay of turbulence behind a heated grid in a wind tunnel is also determined by the small changes in Pe_λ (Re_λ) in the considered range of distances.

Figure 11a shows calculated and experimental normalized correlation functions $f(r)$. The agreement of the obtained data can be considered satisfactory (some other examples, in which the calculation results and experimental data are in good agreement are given in [3, 4, 7, 8, 16]).

Figure 11b presents the calculation results for normalized correlation functions $m(r)$. It is evident that the calculated and measured functions are in sufficiently good agreement. The calculation results obtained for $æ_2 = 0.125$ (they are not shown in Fig. 11) are more consistent with the experimental data. However, in this case, there are significant deviations of the calculated and measured values θ (Fig. 8b).

In the course of numerical experiments, the behavior of the values $\Lambda(t) = \int_0^\infty r^4 B_{LL}(r,t)dr$ (Loitsiansky invariant) and $K(t) = \int_0^\infty r^2 B_{\theta\theta}(r,t)dr$ (Corrsin invariant) was also analyzed. In the numerical solution, the values of these quantities remain constant, i.e., $L(t) = 5.235 \times 10^{-5}$ and $K(t) = 1.247 \times 10^{-3}$. Thus, the calculation results do not contradict the hypothesis of the existence of finite nonzero Loitsiansky and Corrsin invariants. As has already been noted, the issue of the Loitsiansky invariant in the numerical experiments based on the closed Karman–Howarth equation (21) was discussed in detail in [16, 57].

CONCLUSIONS

A closure of the Corrsin equation is performed using the gradient hypothesis connecting the multivariate two-point correlation moment of the third order with the second-order two-point correlation function of a passive scalar field. A numerical model of the locally isotropic turbulence is constructed based on a closed system of Kolmogorov and Yaglom equations. The calculation results for the structure functions D_{LL}, $D_{LL,L}$, $D_{\theta\theta}$, and $D_{L\theta,\theta}$ and the one-dimensional spectra of the fields of the velocity and the passive scalar are in good agreement with the known experimental data. Under the assumption of the constant Loitsiansky and Corrsin invariants, a self-similar solution of the Corrsin equation is constructed, corresponding to the infinite Reynolds and Peclet numbers. A numerical model of the dynamics of turbulence and temperature fluctuations behind a heated grid in a wind tunnel is developed, based on the closed Karman–Howarth and Corrsin equations. The calculation results obtained with the help of it are in good agreement with the available experimental data.

ACKNOWLEDGMENTS

The authors dedicate this work to the blessed memory of Yu.M. Lytkin and V.A. Kostomakha.

This work was supported by the Russian Foundation for Basic Research, project nos. 09-05-01149 and 10-01-00435 and by the Siberian Branch of the Russian Academy of Sciences, SB RAS project no. 23; joint integration project no. 103 of the Siberian, Ural, and Far East Branches of the Russian Academy of Sciences.

REFERENCES

1. A. S. Monin and A. M. Yaglom, *Statistical Fluid Mechanics,* 2nd ed., Vol. 2 (Gidrometeoizdat, St. Petersburg, 1996) [in Russian].
2. K. Hasselmann, "Zur Deutung Der Dreifachen Geschwindigkeits Korrelationen Der Isotropen Turbulenz," *Dtsh. Hydrogr. Zs*, No. 11, 207 (1958).
3. V. A. Kostomakha, "Experimental Simulation of the Isotropic Turbulence," in: Time-Dependent Problems of Continuum Mechanics (Dynamics of Continuous Media), Akad. Nauk SSSR, Siberian Branch, Inst. Hydrodyn, No. 70, 92 (1985).
4. V. A. Kostomakha, "Structure of Isotropic and the Locally Isotropic Turbulence" Candidate's Dissertation in Mathematical Physics (Inst. Hydrodyn., Novosibirsk, 1986).
5. M. D. Millionshchikov, "Isotropic Turbulence in the Turbulent Viscosity Field," *J. Exp. Theor. Phys. Lett.* **10** (8), 406, (1969).
6. M. D. Millionshchikov, "Structure of the Turbulent Viscosity Coefficient for Isotropic Turbulence," *J. Exp. Theor. Phys. Lett.*, **11**(5), 203 (1970).
7. Yu. M. Lytkin and G. G. Chernykh, "A Method for the Closure of Karman—Howarth Equation," in *Dynamics of Continuous Media*, No. 27, 124 (Inst. Hydrodyn. Sib. Otd. Akad. Nauk SSSR, Novosibirsk, 1976).
8. Yu. M. Lytkin and G. G. Chernykh, "Calculations of Correlation Functions in Isotropic Turbulence," in *Dynamics of Continuous Media*, No. 35, 74 (Inst. Hydrodyn. Sib. Otd. Akad. Nauk SSSR, Novosibirsk, 1979)
9. G. K. Batchelor and A. A. Townsend, "Decay of Isotropic Turbulence in Initial Period," *Proc. R. Soc.* A193, 539 (1948).
10. A. A. Townsend, *The Structure of Turbulent Shear Flow*, 2nd ed (Cambridge Univ. Press, 1976).
11. J. A. Domaradzki and G. L. Mellor, "A Simple Turbulence Closure Hypothesis for the Triple-Velocity Correlation Functions in Homogeneous Isotropic Turbulence Revisited," J. Fluid Mech. **140**, 45 (1984).
12. N. I. Akatnov, "Closure of Equations of the Second Two-Point Moments Describing the Decay of Isotropic Turbulence," in *Hydrodynamics* (LGTU, Leningrad, 1990), pp. 31–39.

13. N. I. Akatnov and E. N. Bystrova, "Calculations of Some Characteristics of Homogeneous Turbulence Based on the Solutions of the Karman–Howarth Equation Closed by a Semi-Empirical Model," *Teplofiz. Vys. Temp.* **37** (4), 895 (1999).
14. M. Oberlack and N. Peters, "Closure of the Two-Point Correlation Equation as a Basis for Reynolds Stress Models," *Appl. Sci. Res.*, No. 51, 533 (1993).
15. A. T. Onufriev, "*Description of Turbulent Transport. Nonequilibrium Model. Tutorial*," (Fiz. Tekh. Inst., Moscow, 1995).
16. G. G. Chernykh, Zh. L. Korobitsina, and V. A. Kostomakha, "Numerical Simulation of Isotropic Turbulence Dynamics," *Int. J. Comp. Fluid Dyn.* **10** (2), 173 (1998).
17. S. C. Ling and T. T. Huang, "Decay of Weak Turbulence," *Phys. Fluids*, No. 13, 2912 (1970).
18. M. D. Millionshchikov, "Decay of Homogeneous Isotropic Turbulence in a Viscous Incompressible Fluid," *Dokl. Akad. Nauk SSSR* **22** (5), 236 (1939).
19. L. G. Loitsyanskii, " Some Basic Regularities of an Isotropic Turbulent Flow," *Tr. TsAGI*, No. 440, 3 (1939).
20. A. T. Onufriev and O. A. Pyrkova, "Problem on Damping of Weak Turbulence in a Homogeneous Isotropic Flow," Preprint 2005–1. (Dolgoprudnii, Moscow Fiz. Tekh. Inst., 2005).
21. A. A. Onufriev, A. T. Onufriev, and O. A. Pyrkova, "Approximate solution of the Problem on the Decay of a Homogeneous Isotropic Turbulence Allowing for the Phenomenon of Intermittency in the Flow. Preprint 2008–1. (Dolgoprudnii, Moscow Fiz. Tekh. Inst., 2008).
22. V. A. Frost, "Calculations of Decay of Isotropic Turbulence Using Hasselmann Approximation," in *Proceedings of the All-Russian Workshop and Seminar "Aerophysics and physical mechanics of classical and quantum systems"* (Inst. Appl. Mech., Moscow, 2008), pp. 171–175.
23. V. N. Grebenev and M. A. Oberlack, "Geometric Interpretation of the Second-Order Structure Function Arising in Turbulence," Mathematical Physics, Analysis and Geometry **12** (1), 1 (2009).
24. G. I. Barenblatt and A. A. Gavrilov, "On the theory of self-similar decay of homogeneous isotropic turbulence." *J. Exp. Theor. Phys.* **38** (2), 399 (1974).
25. A. I. Korneyev and L. I. Sedov, "Theory of Isotropic Turbulence and Its Comparison with Experimental Data," *Fluid Mech. Sov. Res.*, No. 5, 37 (1976).
26. U. Shumann and J. Patterson, "Numerical Study of Pressure and Velocity Fluctuations in Nearly Isotropic Turbulence," *J. Fluid Mech.* No. 88, 685 (1978).
27. W. George, "The Decay of Homogeneous Isotropic Turbulence," *Phys. Fluids*, No. A4, 1492 (1992).
28. C. Speziale and P. Bernard, "The Energy Decay in Self-Preserving Isotropic Turbulence Revisited," *J. Fluid Mech.* **241**, 645 (1992).
29. J. Chasnov, "Computation of the Loitsiansky Integral in Decaying Isotropic Turbulence," *Phys. Fluids* **5** (11), 2579 (1993).
30. N. Mansour and A. Wray, "Decay of Isotropic Turbulence at Low Reynolds Number," *Phys. Fluids* **6** (2), 808 (1994).
31. O. Metais and M. Lesieur, "Spectral Large-Eddy Simulation of Isotropic and Stably Stratified Turbulence," *J. Fluid Mech.* **239**, 157 (1992).
32. S. Corrsin, "The Decay of Isotropic Temperature Fluctuations in an Isotropic Turbulence," *J. Aeronaut. Sci.* **18** (12), 417 (1951).
33. R. R. Mills and A. L. Kistler, V. O'Brien, and S. Corrsin, Turbulence and temperature fluctuations behind a heated grid, *NACA Tech. Note No. 4288* (1958).
34. Z. Warhaft, "Passive Scalars in Turbulent Flows," Annu. Rev. Fluid Mech. **32**, 203 (2000).
35. R. A. Antonia, R. J. Smalley, T. Zhou, F. Anselment, and L. Danaila, "Similarity Solution of Temperature Structure Functions in Decaying Homogeneous Isotropic Turbulence," Phys. Rev. E: **69**, 016305–1 (2004).
36. N. I. Akatnov and E. N. Bystrova, "Using an Axisymmetric Model of Turbulence for the Calculation of Statistical Characteristics of the Oscillatory motion in the Flow with a Uniform Constant Shear Rate of the Mean Motion," *Teplofiz. Vys. Temp.* **38** (4), 600 (2000).
37. V. A. Frost, N. N. Ivenskikh, and V. P. Krasitskii, "The Problem of Stochastic Description of Turbulent Micromixing and Combustion on the Base of Two-Point Probability Distribution Functions," Preprint No. 699 (Moscow Inst. for Problems in Mechanics, Russian Academy of Sciences, 2002).
38. V. A. Babenko and V. A. Frost, "Dependence of the Scalar Dissipation on Chemical Transformations in Turbulent Flows," Preprint No. 840 (Moscow Inst. Applied Mechanics, Russian Academy of Sciences, 2007).
39. V. P. Krasitskii and V. A. Frost, "Molecular Transport in Turbulent Flows," Izv. Akad. Nauk, Ser. Mekh. Zhidk. Gaza, No. 2, 190 (2007).
40. V. A. Babenko and V. A. Frost, "Modeling of Turbulent Reacting Flows on the Base of Equation for Scalar Field Correlational Function," *Int. J. Heat Mass Transfer* **52** (13–14), 3314 (2009).
41. M. K. Baev and G. G. Chernykh, "Numerical Modeling of a Turbulent Flow behind a Heated Grid," *Prikl. Mekh. Tekh. Fiz.* **50** (3), 118 (2009).

42. M. K. Baev and G. G. Chernykh, "On Corrsin Equation Closure," *J. of Eng. Thermophys.* **19** (3), 154 (2010).
43. A. N. Kolmogorov, "Energy Scattering under Locally Isotropic Turbulence," *Dokl. Akad. Nauk SSSR* **32** (1), 19 (1941).
44. A. M. Yaglom, "Local Structure of a Temperature Field in a Turbulent Flow," *Dokl. Akad. Nauk SSSR* **69** (6), 743 (1949).
45. Y. Zhu, R. A. Antonia, and I. Hosokava, "Refined Similarity Hypotheses for Turbulent Velocity and Temperature Fields," *Phys. Fluids* **7** (7), 1637 (1995).
46. R. A. Antonia, Y. Zhu, F. Anselment, and M. Ould-Rous, "Comparison Between the Sum of Second-Order Velocity Structure Functions and the Second Order Temperature Structure Function," *Phys. Fluids* **8** (11), 3105 (1996).
47. S. G. Saddoughi and S. V. Veervalli, "Local Isotropy in Turbulent Boundary Layers at High Reynolds Number," *J. Fluid Mech.* **268**, 333 (1994).
48. C. H. Gibson and W. H. Schwarz, "The Universal Equilibrium Spectra of Turbulent Velocity and Scalar Fields," *J. Fluid Mech.* **16** (3), 365 (1963).
49. B. P. Demidovich, I. A. Maron, and E. Z. Shuvalova, *Numerical Methods of Analysis* (GIFML, Moscow, 1963).
50. Yu. S. Zav'yalov, B. I. Kvasov, and V. L. Miroshnichenko, *Methods of Spline Functions* (Nauka, Moscow, 1980) [in Russian].
51. V. F. Demin, L. V. Dobrolyubov, and V. A. Stepanov, *ALGOL Programming Systems* (Nauka, Moscow, 1977) [in Russian].
52. G. S. Golitsyn, "Turbulence Structure in the Area of Small Scales," *Prikl. Mat. Mekh.* **24** (6), 1124 (1960).
53. K. R. Sreenivasan, "On Local Isotropy of Passive Scalars in Turbulent Shear Flows," Proc. R. Soc. London, Ser. A **434**, 165 (1991).
54. L. G. Loitsyanskii, *Fluid and Gas Mechanics* (Nauka, Moscow,1970) [in Russian].
55. L. I. Sedov, *Methods of Similarity and Dimensionality in Mechanics* (Nauka, Moscow,1977) [in Russian].
56. L. D. Landau and E. M. Lifshits, *Hydrodynamics,* 3rd rev. ed. (Nauka, Moscow,1986) [in Russian].
57. U. A. Klimentenok, J.L. Korobitsina, and G. G. Chernykh, "About numerical realization of Loitsiansky-Millionshchikov for asymptotic solution," Mat. Model. **7** (1), 69 (1995).
58. P. A. Davidson, "Was Loitsyansky Correct? A Review of Arguments," J. Turb. No. 1 (2000). http://jot.iop.org.
59. V. N. Grebenev and M. Yu. Filimonov, "Conservation of the Loitsiansky Invariant in the Model of Homogeneous Isotropic Turbulence," *Vestnik Novosibirsk Univ.: Math., Mekh., Inf.* **14** (4), 28 (2009).
60. A. A. Samarskii, *Introduction to the Theory of Difference Schemes* (Nauka, Moscow,1971) [in Russian].